Influence of short-range interactions on the mesoscopic organization of magnetic nanocrystals

Y. Lalatonne, L. Motte, J. Richardi, and M. P. Pileni*
Université Pierre et Marie Curie, Laboratoire des Matériaux Mesoscopiques et Nanométriques U.M.R. 7070, BP 52, 4 place Jussieu, 75005 Paris, France
(Received 15 June 2004; published 18 January 2005)

Magnetic fluids of 10-nm maghemite, γ-Fe_2O_3, nanocrystals, subjected or not to an applied field parallel to the substrate, produce, after evaporation, mesoscopic structures. These differ markedly with the surface coating agent used to prevent particles from coalescence. Citrate ions and carboxylic acids with different chain lengths are employed as coating agents. The change in the mesoscopic structure is studied both experimentally and theoretically. The mesoscopic structures obtained by Brownian dynamics simulations are in good agreement with the experimental observations. In particular, the appearance of chainlike organizations in spite of the particles being weakly dipolar is explained by an interplay of van der Waals and magnetic dipolar interactions.

DOI: 10.1103/PhysRevE.71.011404 PACS number(s): 82.70.Dd, 81.16.Rf, 75.50.Mm, 61.20.Ja

I. INTRODUCTION

Controlling the self-organization of nanocrystals on a mesoscopic scale is a real challenge [1] and opens a new area of research. In fact, it has been demonstrated in the past few years that the optical, magnetic, and transport properties due to 2D and 3D self-organization of nanocrystals are neither those of the nanocrystal itself nor those of the bulk phase [2]. Collective properties are observed and other intrinsic properties due to the self-organization are expected. Very recently, it has also been demonstrated that self-organization of nanocrystals can be used for colloidal nanolithography [3].

We first showed in 1995 that nanocrystals self-organize in 2D and 3D superlattices [4]. Recently it has been reported that "supra" crystals in fcc structures can be produced on a mesoscopic scale [5,6]. To obtain such assemblies, the size distribution of nanocrystals has to be highly reduced and the particle-substrate interactions must be weak. Other self-organizations such as rings or fingers are produced by hydrodynamic instabilities. Such self-organizations depend neither on the size distribution of nanocrystals and type of material used, nor on the substrate [2]. The organization of superparamagnetic nanocrystals depends on several factors such as evaporation rate and the direction of the magnetic field applied during the deposition process [7]. Furthermore for ferromagnetic nanomaterials with strong dipolar interactions, the particles align themselves in the absence of any applied magnetic field [8]. Similarly, the self-organization of semiconductor CdTe nanocrystals in pearl-necklace aggregates is explained by strong electric dipole interactions [9]. Most theoretical and experimental work has focused on the study of these highly dipolar particles. Recently, it was observed that, in spite of weak dipolar interactions, the application of a magnetic field during the evaporation process leads to the formation of structures on submicron scales. Thus, application of a magnetic field, either parallel or perpendicular to the substrate during evaporation can result in aligning nanocrystals with formation of ribbons [10–13] or of dots and labyrinths [14], respectively.

Here, we investigate the mesoscopic organizations of 10-nm maghemite (γ-Fe_2O_3) nanocrystals, characterized by a weak dipolar moment, and differing by their short-range interactions. This is realized by changing the coating agent used to prevent coalescence of the nanocrystals. The organizations of these nanocrystals are observed experimentally by TEM and SEM and modeled by Brownian Dynamics (BD) simulations. From this study we propose a mechanism for the formation of mesoscopic patterns made of magnetic nanocrystals subjected to a parallel field.

II. EXPERIMENTS

A. Chemicals

Sodium dodecyl sulfate, Na(DS), was from Fluka and iron chloride, $Fe(Cl)_2$, and dimethylamine, $(CH_2)_2NH_2OH$, were from Merck. Sodium citrate, $Na_2C_6O_2H_5$, and carboxylic acids $C_nH_{2n+1}COOH$, propanoic acid, C_2H_5COOH, octanoic acid, $C_7H_{15}COOH$, decanoic acid, $C_9H_{19}COOH$, and dodecanoic acid, $C_{11}H_{23}COOH$, were from Aldrich and nitric acid, HNO_3, was from Prolabo. The solvents used, acetone, ethanol, and cyclohexane, were from Fluka. Iron dodecyl sulfate, $Fe(DS)_2$, was made as described in Ref. [15].

B. Apparatus

A Jeol (100 kV) model JEM 100 CX II Transmission Electron Microscope (TEM) and a Jeol model JSM-840A Scanning Electron Microscope (SEM) were used for the characterization of ferrite nanoparticle organizations.

III. SYNTHESIS, CHARACTERIZATION, AND DEPOSITION OF MAGHEMITE, γ-Fe_2O_3, NANOCRYSTALS

10-nm γ-Fe_2O_3 nanocrystals are prepared making a slight change in the synthesis described previously [12] : dimethylamine $[(CH_3)_2NH_2OH]$ is added to an aqueous solution of ferrous dodecyl sulfate $[Fe(DS)_2]$. After mixing the reac-

*Author to whom correspondence should be addressed. Electronic address: pileni@sri.jussieu.fr

tants, the final concentrations are 1.3×10^{-2} mol l^{-1} and 8.5×10^{-1} mol l^{-1} for $Fe(DS)_2$ and dimethylamine, respectively. The solution is stirred vigorously for 2 h at 28.5 °C and the resulting precipitate is isolated from the supernatant by centrifugation. At this stage, uncoated γ-Fe_2O_3 nanocrystals are produced. Two different procedures are used to coat the nanocrystals.

(i) Coating with carboxylic acids ($C_nH_{2n+1}COOH$) with different alkyl chain lengths ($n=2$, $n=7$, $n=9$, and $n=11$): the precipitate of uncoated nanocrystals is washed with a large excess of ethanol. Then, a solution of carboxylic acid solubilized in ethanol ($[C_nH_{2n+1}COOH]=1.4\times10^{-1}$ mol l^{-1}) is added. The solution is subjected to sonication for two hours at 90 °C. The resulting precipitate is washed with a large excess of ethanol and the powder is dried in air. The nanocrystals coated with propanoic acid (C3) are dispersed in water whereas with octanoic acid (C8), decanoic acid (C10), or dodecanoic acid (C12) as coating agent, the nanocrystals are dispersed in cyclohexane. Thus aqueous and organic ferrofluids are obtained.

(ii) Coating with citrate ions. The precipitate is washed with HNO_3 (10^{-2} mol l^{-1}) until a solution of pH=2 is reached. Sodium citrate dissolved in water ($[Na_3C_6O_7H_5]=1.5\times10^{-2}$ mol l^{-1}) is then added to the solution. The mixture is subjected to sonication for 2 h at 90 °C and acetone addition induces nanocrystal precipitation. After washing with a large excess of acetone, the precipitate is dried in air. The nanocrystals coated with citrate ions are dispersed in water.

In order to allow unstable nanocrystals to settle out, all the solutions are kept on a magnet for 12 h, and the supernatant is then collected. A drop of the solution is deposited on a TEM grid with a filter paper underneath. The solution migrates from the substrate to the filter paper and after a few seconds the solvent is totally evaporated. The TEM images (Fig. 1) show that the nanocrystal diameters remain the same whatever the coating is. The average diameter ($d=10$ nm) and the standard deviation ($\sigma=20\%$) are obtained by simulation of the diameter distribution with a log-normal function. Hence the syntheses, described above, provide γ-Fe_2O_3 nanocrystals with various surface coatings and with the same average size (10 nm). X-ray diffraction lines indicate an inverted spinel phase for all the coated nanocrystals with a lattice constant of 0.8360 nm, which is characteristic of γ-Fe_2O_3. The magnetic properties of these nanocrystals dispersed in a nonmagnetic matrix, at a very low weight fraction (0.5%), determined at 3 K by SQUID, are unchanged. The reduced remanence, saturation magnetization, and coercive field are 0.30, 77 A m^2 kg^{-1}, and 2.86×10^4 A m^{-1}, respectively [16]. This indicates that the nanocrystals with different surface coatings have the same magnetic dipole moments. Hence depending on the coating agent, hydrophilic (citrate ions and propanoic acid) and hydrophobic (octanoic, decanoic and dodecanoic acid) magnetic fluids are obtained. For simplicity, let us call nanocrystals coated with citrate ions, propanoic, octanoic, decanoic, and dodecanoic acid, Cit, C3, C8, C10, and C12, respectively.

The nanocrystals are deposited by evaporation of the ferrofluids, subjected or not to a magnetic field (47

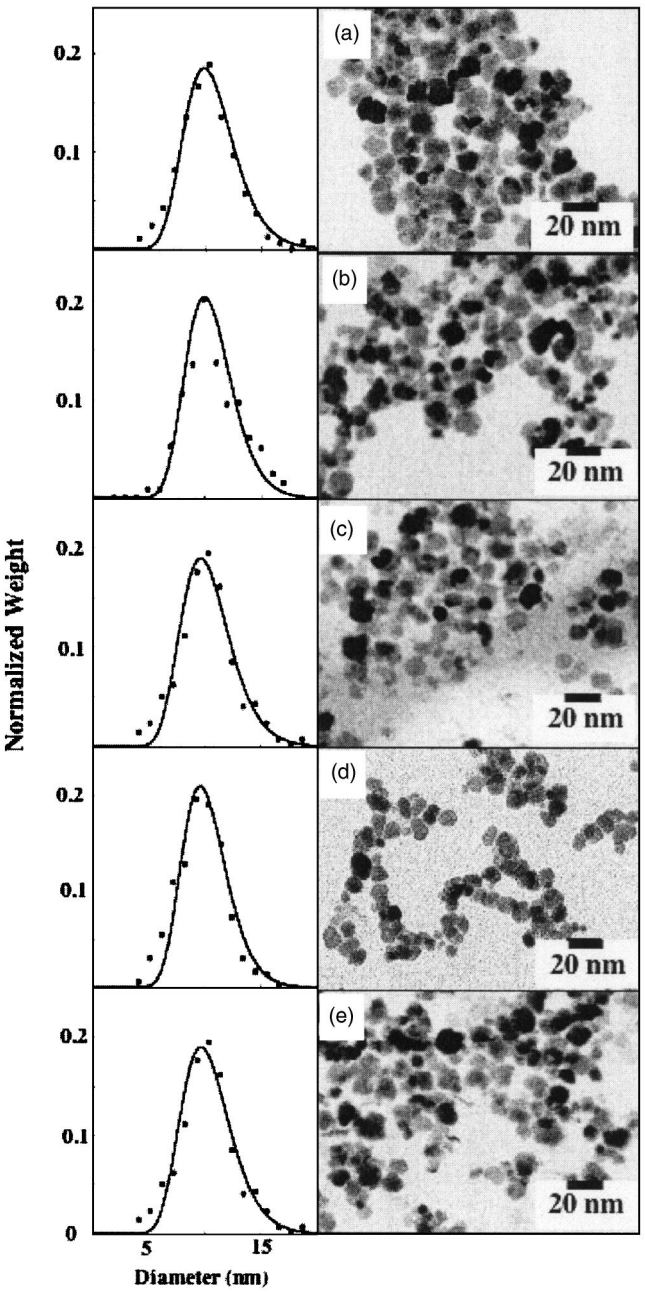

FIG. 1. Diameter histograms and TEM images for randomly deposited γ-Fe_2O_3 nanocrystals with different surface coatings. Nanocrystal surfaces are coated with citrate ions (a), propanoic acid (b), octanoic acid (c), decanoic acid (d), and dodecanoic acid (e).

$\times10^4$ A m^{-1}) parallel to the substrate. Depending on the nanocrystal concentration used for the deposition, the final organizations on the substrates are visualized with TEM (diluted solution) and SEM (concentrated solution). The nanocrystal concentration differs with the deposition mode (see below). The substrates are either a TEM grid covered with amorphous carbon, or HOPG.

Because of the differences in the solvent wetting on the substrates, the nanocrystal deposition procedure differs.

(i) With C8, C10, C12 nanocrystals dispersed in cyclohexane, the substrate is directly dipped in 200 μl of solution and evaporation takes place in a quasisaturated atmosphere.

The evaporation time is 8 h and corresponds to an evaporation rate of 10^{-9} nm ps^{-1}. The initial nanocrystals concentration is either 1.6×10^{-8} mol l^{-1} or 6.2×10^{-6} mol l^{-1}. During the evaporation, the nanocrystals stick to the glass box inducing a loss of particles deposited on the substrate. After the evaporation, nanocrystals staying in the box are dispersed again in cyclohexane. The amount of material deposited on the substrate is deduced by measuring the optical density of this solution.

(ii) With Cit and C3 nanocrystals dispersed in aqueous solutions, the drops remain on the substrate. For the diluted case, one drop (5 μl) of solution containing 3.1×10^{-8} mol l^{-1} of nanocrystals is deposited on the TEM grid. In contrast, for the concentrated case, seven 10 μl volumes of solution containing 6.2×10^{-7} mol l^{-1} of nanocrystals are deposited on the HOPG substrate. The solvent evaporation times are 1 and 8 h, respectively.

By use of the procedures described above, 0.15 μg and 0.45 mg of γ-Fe_2O_3 nanocrystals with different surface coatings are deposited on TEM and SEM substrates, respectively.

IV. SIMULATION METHODS AND INTERACTION MODEL

Langevin equations are used to describe the translation and rotation of the magnetic particles:

$$\frac{\partial \vec{p}_i}{\partial t} = -\zeta_t \vec{p}_i + \vec{F}_i + \vec{F}_{r,i}, \tag{1}$$

$$\frac{\partial \vec{L}_i}{\partial t} = -\zeta_r \vec{L}_i + \vec{T}_i + \vec{T}_{r,i}, \tag{2}$$

where $\vec{p}_i$, $\vec{L}_i$, $\vec{F}_i$, $\vec{T}_i$, ζ_t and ζ_r are the linear and angular momentum of particle i, the force and torque acting on the particle and the friction coefficients, respectively. The two latter values are calculated from Stoke's law using a viscosity of 10^{-3} kg m^{-1} s^{-1} [17]. The random force and torque $\vec{F}_{r,i}$ and $\vec{T}_{r,i}$ are calculated from a Gaussian distribution as usual [18]. The Langevin equations are integrated using an algorithm proposed by Allen [19], which is equivalent to that introduced by van Gunsteren and Berendsen [20,21]. Details of the calculations of forces and torques are given in Ref. [22]. The interparticle interaction is cut off at half the box length. The numbers n of particles used for the simulations are 125 and 512 and the box lengths are fixed at 160 nm for $n=125$ and 320 nm for $n=512$. The time step for the simulations is 20 ps.

The particle-particle interaction is a sum of the terms due to the steric repulsion u_{sr}, the dipole-dipole potential u_{dd}, and the van der Waals (vdW) attraction u_{vdW} [23] :

$$u_{tot} = u_{sr} + u_{vdW} + u_{dd}. \tag{3}$$

The steric repulsion between two particles i and j is described by a model proposed in Ref. [17]:

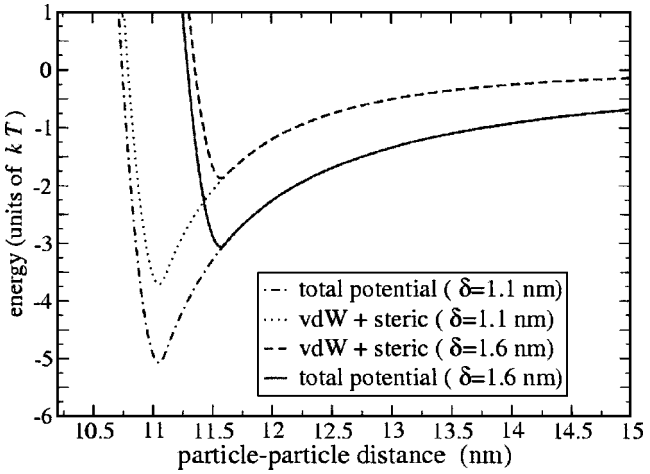

FIG. 2. (Color online) Dependence of the interaction energy on the interparticle distance. The total energy and the sum of the van der Waals attraction and the steric repulsion are shown for two values of the surfactant layer thickness δ. For the calculation of the dipolar interaction, the most stable head-tail configuration is chosen. (Parameters: $A=10^{-19}$ J, $N=5\times10^{18}$ molecules m^{-2}, 10 nm, and $m=2.45\times10^{-25}$ V s m.)

$$u_{sr} = \pi d^2 N k T \left\{ 1 - \frac{r_{ij}-d}{\delta} - \frac{r_{ij}}{\delta} \ln\left(\frac{d+\delta}{r_{ij}} \right) \right\}, \tag{4}$$

where N, d, δ, k, and T are the surface density of the surfactant molecules, the particle diameter, twice the thickness of the coating layer surrounding a nanoparticle, the Boltzmann constant and the temperature, respectively. N is fixed at 5×10^{18} molecules m^{-2}. The dipole-dipole potential u_{dd} and the van der Waals (vdW) attraction u_{vdW} are calculated as follows [23]:

$$u_{dd} = \frac{1}{4\pi\mu_0} \left\{ \frac{\vec{m}_i \cdot \vec{m}_j}{r_{ij}^3} - \frac{3}{r_{ij}^5} (\vec{m}_i \cdot \vec{r}_{ij})(\vec{m}_j \cdot \vec{r}_{ij}) \right\}, \tag{5}$$

$$u_{vdW} = -\frac{A}{12} \left\{ \frac{d^2}{(r_{ij}^2 - d^2)} + \frac{d^2}{r_{ij}^2} + 2 \ln\left(\frac{r_{ij}^2 - d^2}{r_{ij}^2} \right) \right\}. \tag{6}$$

The magnetic moment, m, is calculated from the bulk magnetization (3.73×10^5 A m^{-1}). The average diameter of the nanoparticles is 10 nm and μ_0 is the magnetic permeability. The Hamaker constant A of the ferrite bulk material, 10^{-19} J, is taken from the literature [17]. The BD simulations are carried out varying δ from 1 nm to 3 nm. Figure 2 shows the variation of the intermolecular potential for the most stable head-tail configuration, with and without the dipole term, for $\delta=1.1$ nm and 1.6 nm. For the δ values of 1.1, 1.2, 1.3, and 1.6 nm, the minima of the total potential are −5.1, −4.5, −4.0, and −3.0 in units of kT, respectively. The corresponding minima of the sums of van der Waals and steric interactions are −3.7, −3.2, −2.7, and −1.9 in units of kT, respectively. This shows that the large variation in the total potential is mainly due to the decrease in the van der Waals potential. The dipole potential is less sensitive to the change of interparticle distance. Note that the positions of the

minima, corresponding to the edge-edge core spacing between the particles, are close to δ.

When particles are subjected to an applied magnetic field, H_0, in the direction from the left to the right side of the simulation box, an additional Zeeman term has to be taken into account for the calculation of torques [22] :

$$u_H = -\vec{m}_i \cdot \vec{H}_0. \tag{7}$$

In order to study the influence of the increase in the concentration during evaporation, the following simulations are carried out. The simulation methods differ with the initial nanocrystal concentration.

(i) In the case of diluted solutions, the particles are confined between the substrate and the liquid-gas interface located at the bottom and the top of the simulation box. Periodic boundary conditions are applied only in the directions perpendicular to the substrate. The evaporation process is described by a slow reduction of the gas-solution interface, which decreases with a rate of 10^{-6} nm ps^{-1}. This evaporation rate is slow enough to allow the motion of particles due to diffusion. Thus, the average time for an isolated particle to diffuse from one box side to the other (320 nm for 512 particles) is about 0.4 ms. This is close to the time taken for the simulation of the evaporation.

The substrate and the liquid-gas interface are modeled as follows: the interaction between the substrate and the coated particles is defined as the sum of a steric repulsion term due to the coating and of a van der Waals interaction between the particles themselves and the wall. The potential between a sphere and a half-plane is used to calculate the vdW attraction [24]. The small Hamaker constant of 10^{-20} J used for the vdW term avoids a too large attraction between particle and substrate. When the particle is crossing the gas-liquid interface at the top of the box, the energy increases due to a larger interface. This energy increase of particle i is calculated from the equation

$$\Delta u_i = 2\pi\sigma_{gc} a_p (a_p - d_{gp}) + \pi\sigma_{gs}(a_p^2 - d_{gp}^2),$$

$$\text{where} \quad a_p = (d+\delta)/2 > d_{gp}. \tag{8}$$

d_{gp} is the distance between the center of the particle and the gas-solution interface. For the gas-coating and gas-solvent interface tensions, σ_{gp} and σ_{gs}, we used the same value of 18×10^{-3} J m^{-2}, which is characteristic of organic solvents [24]. The first term corresponds to the energy due to the interface between the particle coating and the gas phase. The second term is caused by the decrease in the solvent-gas interface due to the crossing of the interface by the particle. When the particle crosses the interface, the interfacial area and, therefore, its energy increase due to the energy term in Eq. (8). This energy increase confines the particles in the solution layer.

(ii) When a concentrated solution is used for the nanoparticle deposition, a thick film with an internal three-dimensional structure is experimentally observed after evaporation. A direct simulation of the thick layer of the nanoparticle solution is impossible due to the large number of particles necessary to do so. Therefore, the simulation models only a small cube within the middle of the film of the nanoparticle solution. We assume that the existence of the substrate and gas-liquid interface does not influence the organization and neglect both. Periodic boundary conditions are applied in every spatial direction. To avoid an anisotropic quenching of the structures, the evaporation process is described by a decrease in the box length in all three spatial directions. The particle concentrations locally increase at the boundary of the box due to its shrinking. To avoid this, the particles are homogeneously shifted in the direction of the box center. For this, the particle positions were recalculated every 1000 steps using

$$\Delta\vec{r}_i = \frac{1}{2}\frac{\vec{r}_i - \vec{r}_c}{l_{box}}\Delta l_{box}, \tag{9}$$

where l_{box} and $\vec{r}_c$ are the box length and the vector of the box center. Δl_{box} is the decrease in the box length during 1000 steps. Due to the marked decrease in the box size during the simulation, the spherical cutoff of interactions should especially modify the long-range dipolar forces. Therefore, the Ewald method is used to take the long-range dipolar interaction into account [25,26] ($\alpha = 6.5/l_{box}$; number of k vectors using a spherical cutoff: 709). This method has not been used to simulate diluted solutions, since the size of the box perpendicular to the substrate does not change during the simulation. Moreover, only insignificant differences between 125 and 512 particle simulations are found.

V. RESULTS AND DISCUSSION

We first take into account the γ-Fe_2O_3 nanocrystals coated with octanoic, decanoic, and dodecanoic acids and called C8, C10, and C12, respectively. The TEM images with C8 [Fig. 3(a)] show spherical aggregates of nanocrystals indicating that they tend to attract each other. With C10, on a larger scale [Fig. 3(b)], the nanocrystals appear to be randomly deposited. However, high magnification [inset Fig. 3(b)] shows that they tend to aggregate in clusters of around 10 nanocrystals. Conversely, with C12 [Fig. 3(c)], the nanocrystals are randomly deposited on the TEM grid. This is observed for any magnification [inset of Fig. 3(c)]. When nanocrystals are deposited in a 47×10^4 A m^{-1} magnetic field, the TEM patterns also markedly depend on their coatings, as shown in Fig. 4. With C8, the nanocrystals are organized in rather long, chainlike structures, oriented along the direction of the applied magnetic field [Figs. 4(a) and 4(b)]. The maxima of length, average diameter, and distance of the chains are 40 μm, 300 nm, and 3 μm, respectively. C10 nanocrystals form chainlike structures along the applied field [Figs. 4(c) and 4(d)] with a decrease in the average diameter (250 nm) and the distance between the chains (1 μm) compared to those obtained with C8 nanocrystals [Fig. 4(a)]. Note the presence of isolated nanocrystals between the chainlike structures. With C12, the nanocrystals are more or less randomly deposited on the substrate [Figs. 4(e) and 4(f)]. A small number of agglomerated nanocrystals seem to be oriented along the direction of the applied field. The observed particle aggregation without a magnetic field is a

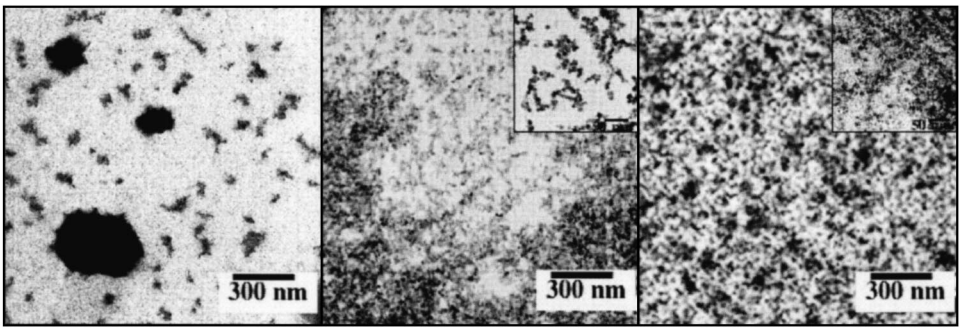

FIG. 3. TEM images of γ-Fe_2O_3 nanocrystals deposited with no magnetic field: C8 (a), C10 (b), and C12 nanocrystals (c).

well-known consequence of the steep distance dependence of the van der Waals interaction. However, the bandlike organization obtained in a magnetic field is rather surprising at submicron scales. To understand these structures, simulations are performed and compared to the experimental images. The existence of chains usually depends on the ratio of the magnetic dipole energy to the thermal energy [23,27–30]:

$$\lambda = \frac{m^2}{4\pi\mu_0(d + d_{ee})^3 kT}, \tag{10}$$

where m, d, and d_{ee} are the particle magnetic moment, the particle diameter, and the edge-edge core spacing, respectively. The edge-edge core spacing between the particles, d_{ee}, depends on the coating of the particles. An estimate of the dipole parameter, λ, for the γ-Fe_2O_3 nanocrystals used in the experiments is obtained from their magnetic moments and size. Neglecting the core spacing, d_{ee}, due to the coating, a value of 0.92 is obtained for λ. Since nonzero values of d_{ee}, expected for coated particles, should lead to smaller λ values according to Eq. (10) , the average dipole parameter of the nanocrystals used is considerably smaller than 0.92. Due to the size dispersion of the particles, even the largest particles of about 15 nm (2% of all particles) have a λ value of 2.6, which is smaller than the threshold λ of about 3 for chain formation [8]. Moreover, a recent simulation study shows that chains of larger dipolar particles do not induce the aggregation of smaller particles in polydisperse systems even in a field [30]. The fact that the structures almost completely disappear with C12 nanocrystals indicates that the dipolar energy between the larger particles is not sufficient to induce aggregation. We conclude that the former calculation of λ cannot be used to explain the chainlike organization experimentally observed here.

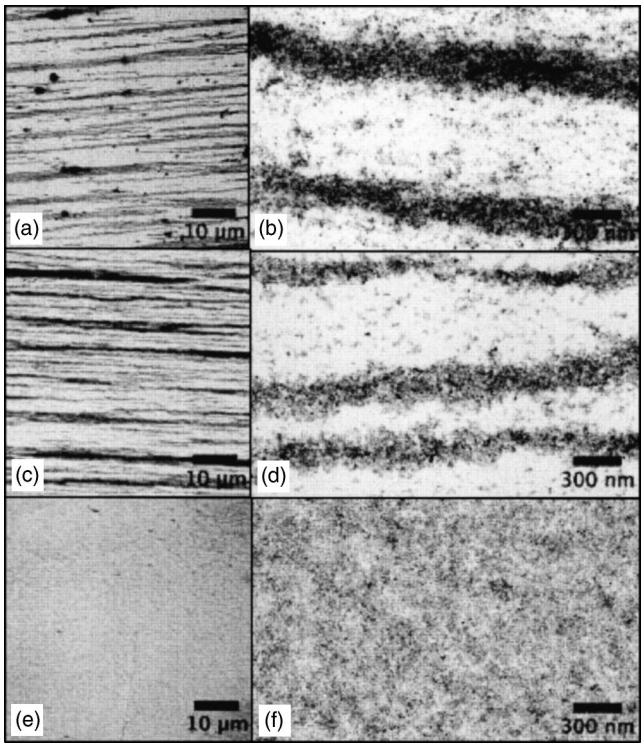

FIG. 4. TEM images obtained at various magnifications for maghemite nanocrystals deposited with a magnetic field: C8 (a, b), C10 (c, d), and C12 nanocrystals (e, f).

At this point, we investigate the stability of the magnetic fluid subjected or not to an applied magnetic field from a theoretical point of view. The evaporation process is neglected. The particle number and the box size used for the simulations are 512 and 320 nm, respectively. This corresponds to a particle concentration (2.6×10^{-5} mol l^{-1}) larger than that used in the initial experiments conditions. Simulations are carried out varying the coating thickness δ from 1 nm to 3 nm. With no applied magnetic field, for δ=3 nm, no particle aggregation is observed. All the other simulations are started from the configuration obtained by this run. The final configurations are obtained after five million time steps for the various δ values. For δ smaller than 1 nm, there are strong attractions between particles with particle aggregation on a large scale. Obviously, the steric repulsion is not sufficient to stabilize the colloidal system. At and above δ =1.1 nm no particle aggregation appears. In a strong applied magnetic field (47×10^4 A m^{-1}) all the magnetic dipoles are oriented in the magnetic field direction and no changes in the initial configuration compared to that obtained without a field are observed. From this it is concluded that the magnetic fluid is stable when the coating thickness is larger than 1 nm.

During the evaporation process, the particle concentration increases. In order to study the influence of the evaporation process, the first method (i) in Sec. IV is used. The simulations are started from the final configurations described above. The configurations obtained after 14 million steps for the various δ values without and with an applied magnetic field are shown in Fig. 5: for δ=1.1 nm and δ=1.2 nm, ag-

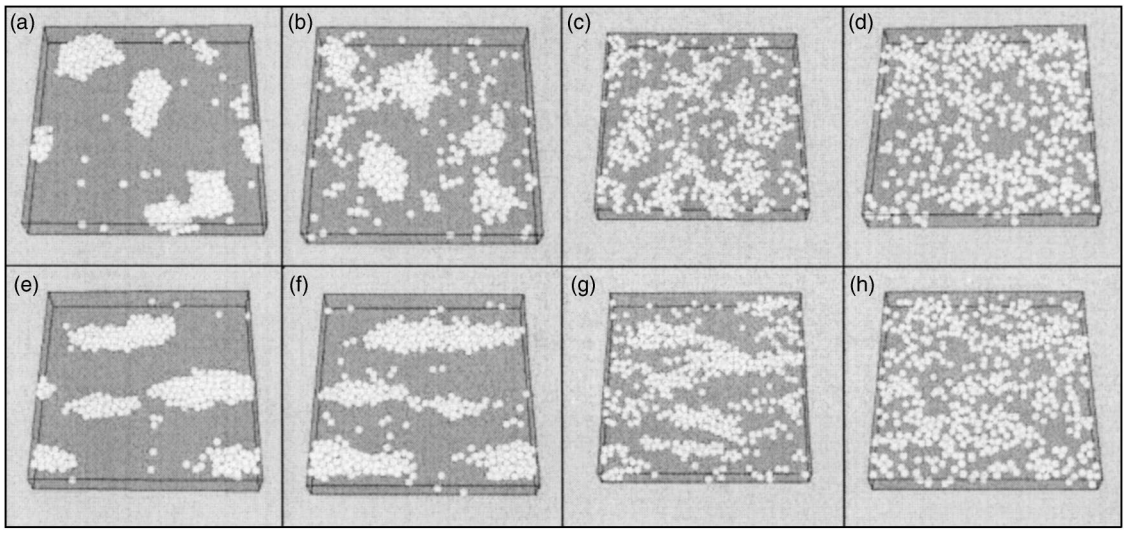

FIG. 5. Snapshots of the configurations of the BD simulations obtained by evaporation of the solvent after 14 million steps. The results for different values of twice the surfactant layer thickness δ are shown. Top: simulations with no field, a (δ=1.1 nm), b (δ=1.2 nm), c (δ=1.3 nm), and d (δ=1.6 nm); bottom: application of a 47×10^4 A m^{-1} magnetic field, e (δ=1.1 nm), f (δ=1.2 nm), g (δ=1.3 nm), and h (δ=1.6 nm). The box length is fixed at 320 nm.

gregates of particles formed during the evaporation process are observed [Figs. 5(a) and 5(b)]. In an applied field the clusters tend to align [Figs. 5(e) and 5(f)]. At δ=1.6 nm, no aggregation of the particles is observed without [Fig. 5(d)] or with [Fig. 5(h)] an applied magnetic field. At δ=1.3 nm, an intermediate behavior is observed with formation of small clusters of particles without [Fig. 5(c)] and not well-defined alignment [Figs. 5(g)] with an applied magnetic field. Above δ=1.4 nm behavior similar to that at δ=1.6 nm is observed.

The evaporation rate used during the simulation is very fast (10^{-6} nm ps^{-1}) compared to the experimental value (10^{-9} nm ps^{-1}), determined by the boiling temperature of the solvent. The evaporation rate is limited by the computation time, since even a simulation of the evaporation with 10^{-6} nm ps^{-1} takes 2 weeks on our computers (Intel Xeon, 2 GHz). This raises a question of the validity of the simulations, since the experimental and simulated evaporation rates markedly differ. To investigate the influence of the evaporation rate on the theoretical results, a systematic simulation study is carried out varying this rate between 2×10^{-7} and 5×10^{-6} nm ps^{-1}. For these simulations, a smaller number of particles are used, which allows a considerable reduction in

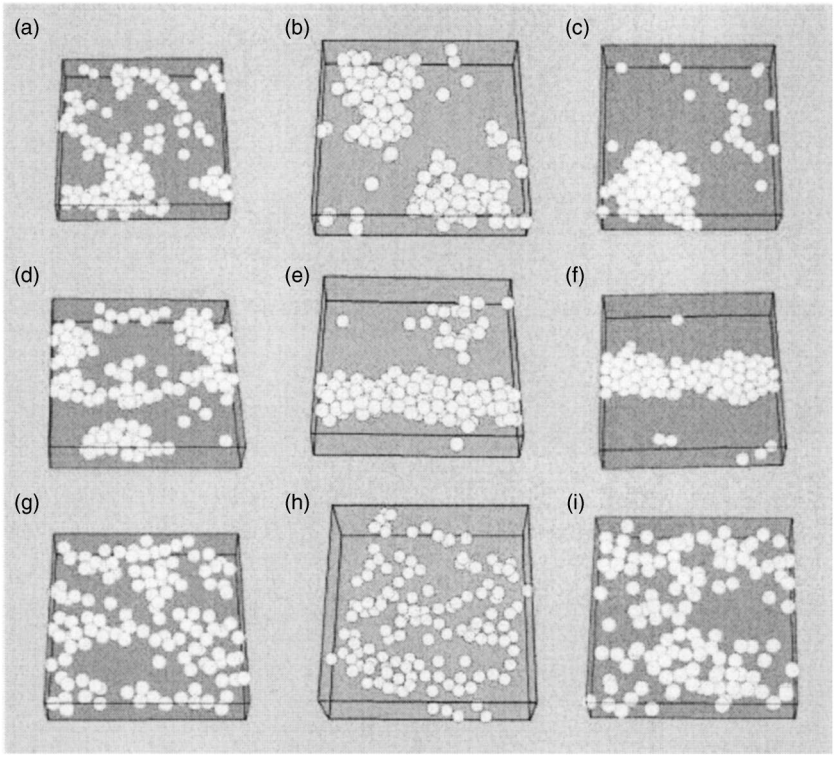

FIG. 6. Snapshots of the configurations of the BD simulations obtained by evaporation of the solvent after 14 million steps. The results for different evaporation rates are shown. Top: simulations with no field, δ=1.2 nm: a (5×10^{-6} nm ps^{-1}), b (10^{-6} nm ps^{-1}), c (0.2×10^{-6} nm ps^{-1}); middle: application of a 47×10^4 A m^{-1} magnetic field, δ=1.2 nm: d (5×10^{-6} nm ps^{-1}), e (10^{-6} nm ps^{-1}), f (0.2×10^{-6} nm ps^{-1}); bottom: application of a 47×10^4 A m^{-1} magnetic field, δ=1.6 nm: g (5×10^{-6} nm ps^{-1}), h (10^{-6} nm ps^{-1}), I (0.2×10^{-6} nm ps^{-1}). The box length is fixed at 160 nm.

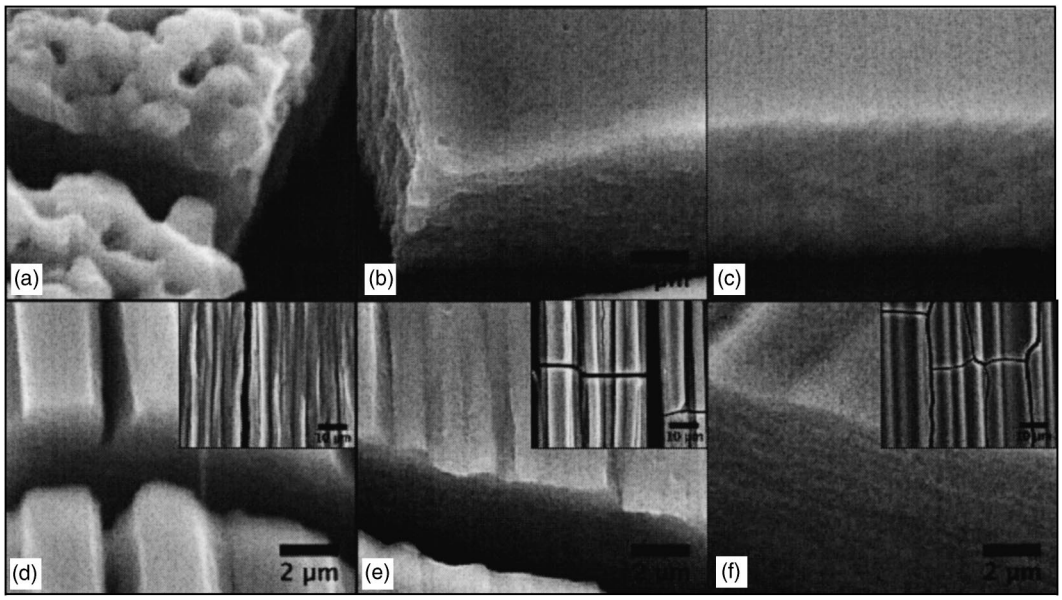

FIG. 7. SEM images of γ Fe_2O_3 nanocrystals deposited with no magnetic field (a: C8; b: C10; c: C12) and with a magnetic field (d: C8; e: C10; f: C12).

the computation time. Let us consider three different evaporation rates (5×10^{-6} nm ps^{-1}, 10^{-6} nm ps^{-1}, 2×10^{-7} nm ps^{-1}) for particles having coating layer thicknesses of 1.2 nm and 1.6 nm and subjected or not to an applied magnetic field (47×10^{4} A m^{-1}). With no applied magnetic field and $\delta=1.2$ nm, the structure is not well organized [Fig. 6(a)] when the evaporation is fast (5×10^{-6} nm ps^{-1}). On decreasing the evaporation rate from 10^{-6} nm ps^{-1} [Fig. 6(b)] to 0.2×10^{-7} nm ps^{-1} [Fig. 6(c)] similar morphologies of the clusters are observed. However, the cluster size increases with decreasing the evaporation rate. In a magnetic field, for any evaporation rate, the particles tend to align. However, as with no applied field [Fig. 6(a)], rather poor organization is found when the evaporation rate is fast [Fig. 6(d)] whereas the particles are well aligned on decreasing the evaporation rate [Fig. 6(e)]. Note that a further decrease in the evaporation rate does not change the particle alignment [Fig. 6(f)]. For a thicker coating layer, the particles subjected to an applied field do not self-organize for any evaporation rate [Figs. 6(g)–6(i)]. This systematic study shows that the evaporation rate used in the simulations is sufficiently low to predict qualitatively the morphologies of organizations.

Qualitatively, the images produced experimentally (Figs. 3 and 4) and from simulation (Fig. 5) show similar structures. Spherical aggregates with no magnetic field [Figs. 3(a) and 5(a)] and elongated structures [Figs. 4(b) and 5(e)] with a field are observed when nanocrystals are coated with short chains. The structures disappear on increasing the thickness of the coating [Figs. 3(c), 5(d), 4(f), and 5(h)]. A quantitative comparison is limited because of the particle number and the evaporation speed used in the simulation. However, a careful study of experimental results obtained with C8 nanocrystals [Figs. 3(a) and 4(a)] and a simulation obtained with $\delta=1.2$ nm [Figs. 5(a) and 5(e)] is made. From experiments, the aggregates size varies from 50 nm to 400 nm [Fig. 3(a)] whereas the simulated size increases from 50 nm to 100 nm [Fig. 5(a)]. In an applied magnetic field, the diameter of elongated structures is around 300 nm from experiments whereas it is 60 nm from the simulation. The experimental data and simulation have the same order of magnitude. However, the simulated values are always smaller than those obtained from experiments. This can be explained by the relatively fast evaporation speed applied in the simulation in comparison with the experiment. Furthermore, the nanocrystal size distribution, which is not taken into account in the simulations, might influence the size of aggregates.

From these data it is concluded that, because the γ-Fe_2O_3 nanocrystals with different surface coatings keep the same average size, crystalline structure (inverted spinel), and magnetic properties, the coating is the major cause of the change in the mesoscopic structures observed in Figs. 3 and 4. Moreover, the magnetic dipolar interactions are too small to induce a self-ordering of the nanocrystals as observed by Philipse *et al.* [8]. With no magnetic field, the aggregations observed with C8 and C10 nanocrystals are caused by vdW interactions and not by a dipolar force, for which more chainlike aggregates are expected. The simulations, shown in Fig. 5, provide evidence that when the distance between particles is short enough, the vdW attraction induces aggregation of particles. In this case, the application of a field leads to chainlike structures, which is observed by experiment [Figs. 4(a)–4(d)] and by simulation [Figs. 5(e) and 5(f)]. This is due to the fact that the application of the field induces a total magnetic dipole in each cluster, which is much larger than that of a single particle. Therefore, the clusters attract each other to form larger elongated aggregates. The marked dependence of the vdW interaction on the interparticle distance explains why a small increase in the alkyl chain length leads to the disappearance of particle aggregation observed in the experiments. The aggregation disappears when the edge-edge core spacing d_{ee} between the particles is varied from 1.3 to 1.4 nm. A similar disappearance of organization is experimentally observed when C12 instead of C10 is used

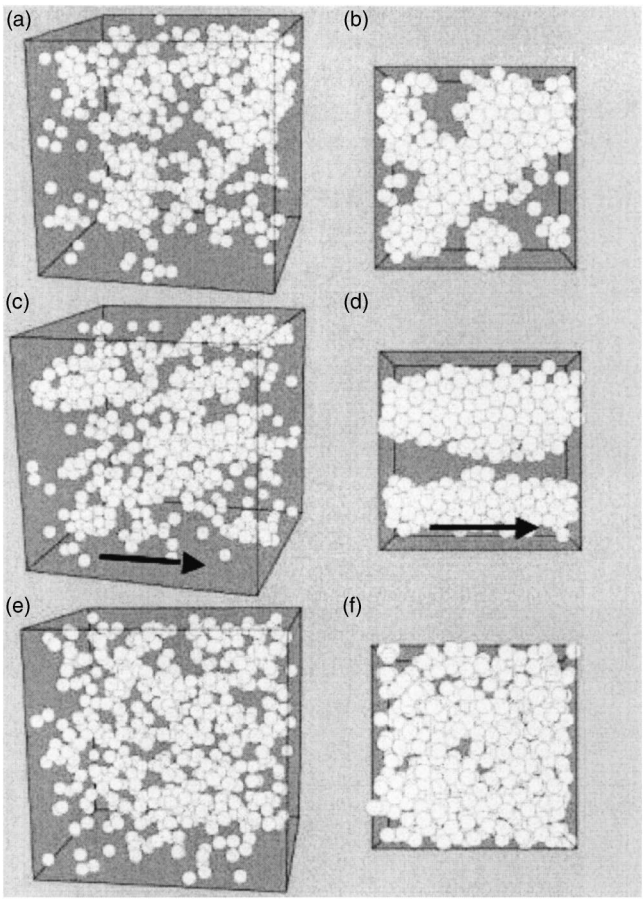

FIG. 8. Snapshots of the configurations after various simulation times. Top: simulations with no field, δ=1.2 nm, a (0.12 ms, box length: 200 nm), b (0.18 ms, box length: 140 nm); middle: application of a 47×10^4 A m^{-1} magnetic field, 1.2 nm, c (0.12 ms, box length: 200 nm), d (0.18 ms, box length: 140 nm); bottom: application of a 47×10^4 A m^{-1} magnetic field, δ=1.6 nm, e (0.12 ms, box length: 200 nm), f (0.18 ms, box length: 140 nm).

as the coating. An evaluation of the interparticle spacings, which can be expected for these coatings, is obtained from Ag_2S nanocrystals coated with alkanethiols and self-assembled in hexagonal networks [31]. Thus, an increase in the core spacing from 1.6 to 1.7 nm is observed in this system, when decanthiol (C10) is replaced by dodecanthiol (C12) as the coating agent. These experimentally observed spacings are in reasonable agreement with the values used here in the simulations. In addition, the increase of 0.1 nm in spacing, experimentally expected between C10 and C12, is similar to the small variation necessary for the disappearance of organization in simulations. The strong vdW attraction between the C8 nanocrystals is supported by the fact that these nanocrystals cannot be solubilized in some organic solvents, such as hexane, in contrast to C10 and C12 nanocrystals. When the distance between nanocrystals increases (C12 nanocrystals), experiments clearly show the randomly deposited nanocrystals without [Fig. 3(c)] and with [Figs. 4(e) and 4(f)] a magnetic field applied during the deposition process.

A question arises: do we keep similar mesostructures when a rather large amount of nanocrystals is deposited on a substrate? To answer this question, experiments similar to those described above are performed. The only change is the concentration of γ-Fe_2O_3 nanocrystals used during the deposition process (6.2×10^{-6} mol l^{-1}). In this case, the samples are studied by scanning electron microscopy (SEM). With no magnetic field, the SEM image with C8 nanocrystals shows a very rough surface [Fig. 7(a)]. The film is made of spherical, highly compact aggregates, with an average diameter of 1.5 ± 1 μm. Conversely with C12, a very flat surface with a high compacity of the film is observed [Fig. 7(c)]. For the intermediate case of C10 nanocrystals, the surface is still somewhat rough, whereas an aggregation is no longer observed [Fig. 7(b)]. In a magnetic field with C8 nanocrystals, there is formation of long cylinders with a very regular structure [inset in Fig. 7(d)]. By tilting the sample, it is seen that the structure corresponds to superimposed cylinders with an average diameter of 3 ± 1 μm [Fig. 7(d)]. With C10 nanocrystals, a marked undulation of the surface is observed [Fig. 7(e)]. The stripes are considerably thinner than those with C8 [Fig. 7(d)]. Conversely, with C12 nanocrystals, the stripes observed on a large scale correspond to a slight undulation at the surface of the film [Fig. 7(f)]. Whatever the coating is, the thickness of the samples varies from 3 μm in the center of the sample to 10 μm in its border. In order to understand formation of three-dimensional structures, we model the evaporation in a small cube within the middle of the nanoparticle solution layer [see evaporation method (ii) in Sec. IV]. Figures 8(a) and 8(b) show the simulation results for δ=1.2 nm after 0.12 ms (box length: 200 nm) and 0.18 ms (box length: 140 nm), respectively. With no magnetic field, particle aggregation is observed. In a magnetic field applied in the arrow direction and for the same δ (1.2 nm) and similar times, the particles tend to align [Figs. 8(c) and 8(d)]. This structure is explained by the same mechanism as the chainlike organization in Figs. 5(f) and 5(e). For simulations in the same conditions at δ=1.6 nm, no structures are observed. From these data, it is concluded that the morphologies of mesostructures obtained experimentally and by simulations agree qualitatively. Moreover, the mesoscopic structures do not depend on the amount of nanocrystals deposited on the substrate and markedly differ with their coating.

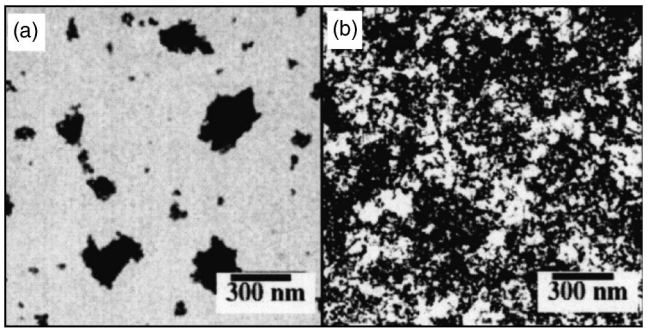

FIG. 9. TEM images of γ-Fe_2O_3 nanocrystals deposited with no magnetic field: cit (a) and C3 nanocrystals (b).

Another question arises: do other types of interactions play similar roles in the mesostructure shape? To answer this question, γ-Fe_2O_3 nanocrystals are coated with a passivating agent allowing them to disperse in aqueous solution. Citrate

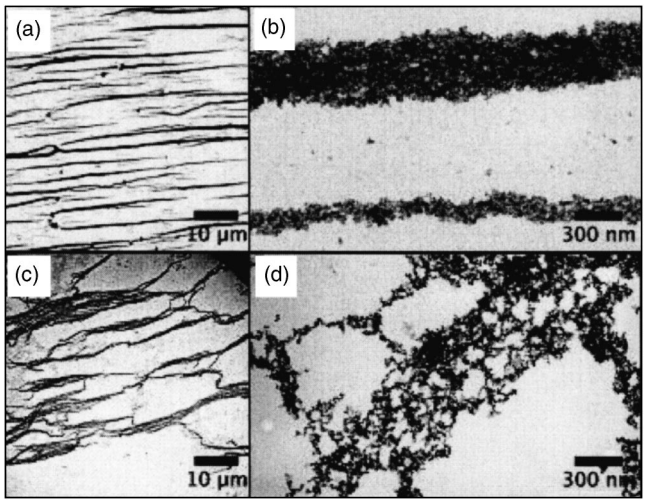

FIG. 10. TEM images obtained at various magnifications for γ-Fe_2O_3 nanocrystals deposited with a magnetic field: cit (a, b) and C3 nanocrystals (c, d).

ions and propanoic acid are used. For simplicity the nanocrystals are called Cit and C3, respectively. The deposition process differs from that used previously (see Sec. III). As above, the solvent is evaporated by applying or not a magnetic field parallel (47×10^4 A m^{-1}) to the substrate. Furthermore, diluted and concentrated solutions of γ-Fe_2O_3 nanocrystals are deposited.

For dilute solutions, with no applied magnetic field, the TEM image obtained after evaporation of Cit nanocrystals shows spherical aggregates of nanocrystals [Fig. 9(a)], as observed above in cyclohexane for C8 nanocrystals [Fig. 3(a)]. Conversely, C3 nanocrystals are randomly deposited on the TEM grid [Fig. 9(b)]. This is observed whatever the magnification. In a magnetic field, the TEM patterns markedly differ. Long chainlike structures are formed with Cit nanocrystals [Figs. 10(a) and 10(b)]. The average length (40 μm), diameter (300 nm), and average distance between the chains (3 μm) are similar to those observed for C8 nanocrystals [Figs. 4(a) and 4(b)]. Note that very few particles are between these ribbons. By replacing Cit with C3 nanocrystals, a drastic change in the self-organization is observed: on a large scale, Figs. 10(c) and 10(d) show interconnected chainlike structures up to 100 μm in length. For concentrated solutions, with Cit nanocrystals, the SEM image shows a very rough surface [Fig. 11(a)] with spherical, highly compact agglomerates, having an average diameter of 1.5 ± 1 μm. Conversely with C3, the SEM pattern shows a very flat surface and high compacity of the film [Fig. 11(b)]. In a magnetic field, Cit nanocrystals self-organize in long cylinders with a very regular structure [inset Fig. 11(c)]. By tilting the sample [Fig. 11(c)], it is seen that the structure corresponds to superimposed tubes with an average diameter of 3 ± 1 μm. Conversely, with C3 nanocrystals, stripes are observed on a large scale with highly dense and undulated structures [inset Fig. 11(d)] and the surface is very flat [Fig. 11(d)]. Hence the SEM images obtained with Cit and C3 are similar to those observed with C8 and C12. Of course, because these nanocrystals are dispersed in aqueous solution, new kinds of interactions such as ionic double layer repulsion and hydrophobic interactions have to be taken into account and the theoretical model developed above cannot be applied directly. Nevertheless, these simulations show that particle aggregation can be expected for these particles having a layer thickness smaller than those of C8 and C10 nanocrystals. For Cit nanocrystals solubilized in water, the distance between the particles is determined by the overlap of the ionic double layers surrounding the particles [24]. During the evaporation the distance between particles should be reduced, since the Debye length markedly decreases with increasing concentration. Therefore, at the end of the evaporation, aggregation can be expected like that observed with

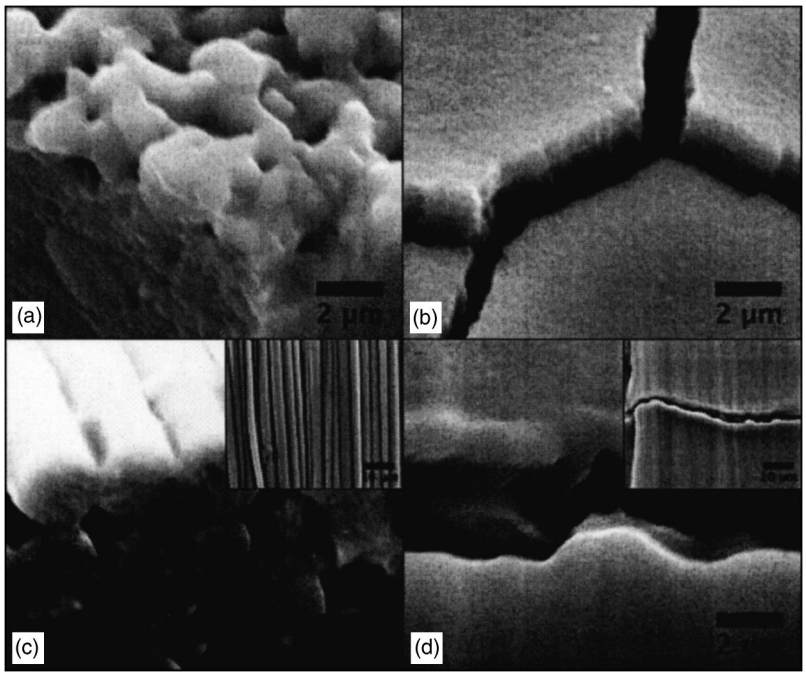

FIG. 11. SEM images of maghemite nanocrystals deposited with no magnetic field (a: cit, b: C3) and with a magnetic field (c: cit, d: C3).

C8 nanocrystals. This is in good agreement with the experiment. The case of C3 nanocrystals seems to be more complicated. No aggregation is observed without a field, while chainlike structures appear when the field is applied during evaporation. This might be a side effect of the hydrophobic interactions expected for this surfactant. For the citrate ions, hydrophobic attraction does not exist, since this coating is highly hydrophilic.

VI. CONCLUSION

Soft chemistry is used to make 10-nm γ-Fe_2O_3 nanocrystals with different surface coatings. Nanocrystals are deposited on a TEM grid and a drastic change in their organization is obtained on varying the coating. When the nanocrystal distance is rather small, as observed with citrate ions, octanoic and decanoic acids as passivating agents, the nanocrystals tend to aggregate without any applied magnetic field, whereas they form ribbons in the direction of an applied field. Particle aggregation is attributed to strong van der Waals attraction. The chainlike mesostructures form in spite of a small magnetic dipole. This can be explained by the combination of van der Waals and dipolar interactions as demonstrated by the simulations in the case of carboxylic acid-coated nanocrystals. The van der Waals interaction is very sensitive to the interparticle distance. This explains the disappearance of any mesostructures, when the surfactant size is increased, as in the case of dodecanoic acid as coating agent. The details of the mesostructures are not yet well understood, in particular, for propanoic acid as coating agent. It will be necessary to develop more complex interaction models taking, e.g., the hydrophobic interaction into account. Moreover, the use of other coating agents, such as hydrophilic nonionic surfactants, could yield valuable additional information.

ACKNOWLEDGMENT

The authors would like to thank Dr. Ngo for fruitful discussions.

[1] G. M. Whitesides and B. Grzybowski, Science **295**, 2418 (2002).
[2] M. P. Pileni, J. Phys. Chem. **105**, 3358 (2001).
[3] D. Ingert and M. P. Pileni, J. Phys. Chem. B **107**, 9617 (2003).
[4] L. Motte, F. Billoudet, and M. P. Pileni, J. Phys. Chem. **99**, 16425 (1995).
[5] A. Courty, C. Fermon, and M. P. Pileni, Adv. Mater. (Weinheim, Ger.) **13**, 254 (2001).
[6] I. Lisiecki, P. A. Albouy, and M. P. Pileni, Adv. Mater. (Weinheim, Ger.) **15**, 712 (2003).
[7] M. P. Pileni, Adv. Funct. Mater. **11**, 323 (2001).
[8] K. Butter, P. H. H. Bomans, P. M. Frederik, G. J. Vroege, and A. P. Philipse, Nat. Mater. **2**, 88 (2003).
[9] Z. Tang, N. A. Kotov, and M. Giersig, Science **297**, 237 (2002).
[10] A. T. Ngo and M. P. Pileni, Adv. Mater. (Weinheim, Ger.) **12**, 276 (2000).
[11] J. Legrand, C. Petit, and M. P. Pileni, J. Phys. Chem. B **105**, 5643 (2001).
[12] A. T. Ngo and M. P. Pileni, J. Phys. Chem. B **105**, 53 (2001).
[13] Y. Lalatonne, J. Richardi, and M. P. Pileni, Nat. Mater. **3**, 121 (2004).
[14] J. Legrand, A. T. Ngo, C. Petit, and M. P. Pileni, Adv. Mater. (Weinheim, Ger.) **13**, 58 (2001).
[15] N. Moumen, P. Veillet, and M. P. Pileni, J. Magn. Magn. Mater. **149**, 67 (1995).
[16] Y. Lalatonne, L. Motte, V. Russier, A. T. Ngo, P. Bonville, and M. P. Pileni, J. Phys. Chem. B **108**, 1848 (2004).
[17] R. E. Rosensweig, *Ferrohydrodynamics* (Cambridge University Press, Cambridge, U.K., 1985).
[18] M. P. Allen and D. J. Tildesley, *Computer Simulation of Liquids* (Clarendon, Oxford, 1987).
[19] M. P. Allen, Mol. Phys. **40**, 1073 (1980).
[20] W. F. van Gunsteren and H. J. C. Berendsen, Mol. Phys. **45**, 637 (1982).
[21] M. P. Allen, Mol. Phys. **47**, 599 (1982).
[22] H. Morimoto and T. Maekawa, J. Phys. A **33**, 247 (2000).
[23] H. Morimoto and T. Maekawa, Int. J. Mod. Phys. B **13**, 2085 (1999).
[24] R. J. Hunter, *Foundations of Colloid Science* (Oxford University Press, Oxford, 2001).
[25] S. W. de Leeuw, J. W. Perram, and E. R. Smith, Proc. R. Soc. London, Ser. A **373**, 27 (1980).
[26] Z. Wang, C. Holm, and H. W. Müller, J. Chem. Phys. **119**, 379 (2003).
[27] R. W. Chantrall, A. Bradbury, J. Popplewell, and S. W. Charles, J. Appl. Phys. **53**, 2742 (1982).
[28] J. J. Weis, Mol. Phys. **93**, 361 (1999).
[29] J. M. Traves, J. J. Weis, and M. M. Telo da Gamma, Phys. Rev. E **59**, 4388 (1999).
[30] Z. Wang and C. Holm, Phys. Rev. E **68**, 041401 (2003).
[31] L. Motte and M. P. Pileni, J. Phys. Chem. B **102**, 4104 (1998).